Journal of Materials Chemistry A

ROYAL SOCIETY OF CHEMISTRY

PAPER

View Article Online
View Journal

Cite this: DOI: 10.1039/d6ta00496b

A PCM-enhanced thermoelectric generator with enhanced power density and lifespan

Xizu Wang,†[a] Wenting Chen,†[ab] Xiang Yun Debbie Soo, †[a] Jinfeng Dong, [d] Xian Yi Tan,[a] Suxi Wang,[a] Warintorn Thitsartarn,[a] Rong Ji,[a] Jianwei Xu,[e] Xian Jun Loh, [a] Yun Zheng, *[c] Hai-dong Yu*[b] and Qiang Zhu *[a]

Waste heat harvesting with thermoelectric generators (TEGs) is fundamentally limited by low conversion efficiency and operational instability, particularly under conditions of fluctuating external temperatures. Here, we propose a novel sandwich-style TEG to achieve high-efficiency waste heat harvesting and conversion. The design is based on a phase change material-integrated thermoelectric generator (PCM-TEG), fabricated by sandwiching TEG modules between two layers of PCMs. This architecture transforms passive thermal storage into active energy conversion, thereby unifying efficient heat management with continuous power generation. The synergistic design addresses long-standing challenges including poor energy conversion efficiency, thermal oxidation, and short discharge duration. By employing thermally conductive electrodes and composite PCMs, the system maintains high thermal storage capacity while enabling stable, long-term electricity output from otherwise wasted heat. Experiments reveal a >100% enhancement in effective power density and a fivefold improvement in output stability and device lifetime. These results establish the PCM-TEG as a promising platform for next-generation thermoelectric battery systems, offering scalable solutions for sustainable energy storage, waste-heat utilization, and thermal insulation technologies.

Received 19th January 2026
Accepted 12th May 2026

DOI: 10.1039/d6ta00496b

rsc.li/materials-a

Introduction

Waste heat from industrial and daily activities represents a largely untapped renewable energy resource with enormous potential.[1] Thermoelectric (TE) technology, exploiting the Seebeck effect, enables direct conversion of heat into electricity.[2,3] Despite decades of progress, practical deployment continues to be restricted by low conversion efficiency and limited durability, particularly when exposed to fluctuating environmental temperatures.[4] Thermoelectric generators (TEGs) have demonstrated considerable potential for harvesting energy from solar,[5] biomass,[6] geothermal,[7] and automotive waste heat.[8] However, their conversion efficiency seldom exceeds 12–14%,[9–11] primarily constrained by the intrinsic figure of merit (ZT) of thermoelectric materials and the magnitude of the accessible temperature gradient.[12] While TEGs offer intrinsic reliability through their solid-state architecture, absence of moving parts, and continuous power output, performance degradation under temperature fluctuations and material aging remains a critical issue.[13] This challenge is exacerbated in variable, low-to mid-temperature environments, where unstable hot-side conditions or inadequate cold-side cooling can drastically reduce output.[14] Skutterudites undergo Sb sublimation above 653 K, causing performance loss.[15] Likewise, Mg volatility leads to evaporation from Mg_3Sb_2-based and Mg_2Si-based compounds.[16,17] Moreover, at service temperatures (~200–300 °C for Bi_2Te_3), ambient exposure further promotes oxidation and electrode diffusion.[18–20] In addition, achieving high and stable power generation below 200 °C across diverse geometries, including wearable and curved configurations, remains a significant challenge. The performance of existing systems is limited by inadequate adaptability to variable heat-collection conditions, pronounced sensitivity to thermal boundary fluctuations, and instability at thermal interfaces.

Current efforts to improve the efficiency of thermoelectric cells have primarily focused on intrinsic semiconductor modification strategies, such as elemental doping[21] and band

[a]Institute of Materials Research and Engineering (IMRE), Agency for Science, Technology and Research (A*STAR), 2 Fusionopolis Way, Innovis #08-03, Singapore 138634, Republic of Singapore. E-mail: zhuq@a-star.edu.sg

[b]State Key Laboratory of Flexible Electronics (LOFE) and Institute of Flexible Electronics (IFE), Shaanxi Key Laboratory of Flexible Electronics, MIIT Key Laboratory of Flexible Electronics (KLoFE), Northwestern Polytechnical University, 127 West Youyi Road, Xi'an 710072, P.R. China. E-mail: iamhdyu@nwpu.edu.cn

[c]Key Laboratory of Optoelectronic Chemical Materials and Devices, Ministry of Education, Jianghan University, Wuhan 430056, P.R. China. E-mail: zhengyun@jhun.edu.cn

[d]School of Materials Science and Engineering, Nanyang Technological University, Singapore 639798, Singapore

[e]Institute of Sustainability for Chemical, Energy and Environment (ISCE2), Agency for Science, Technology and Research (A*STAR), 1 Pesek Road, Jurong Island, 627833, Singapore

† These authors contributed equally to this work.

structure engineering.[22] In contrast, this work presents a novel sandwich-structured TEG for efficient waste heat harvesting and conversion. The device integrates TEG modules with phase change materials (PCMs), embedding the TEG modules between two PCM layers, thereby combining both engineering and materials design perspectives. The novel PCM-TEG represents a "thermal-electric-buffer" integrated system, in which phase change materials serve as thermal reservoirs to provide a continuous and stable heat supply for thermoelectric generators, even under intermittent heat sources. By using thermal energy as the central medium, the novel PCM-TEG integrates heat collection, storage, regulation, and conversion within a highly compact, all-solid-state, and long-lifespan architecture. This system enables the efficient and reliable conversion of unstable, low-grade heat into a stable electrical power output, a capability that conventional systems relying on mechanical conversion or electrochemical storage can scarcely achieve.

In addition, the introduction of PCM structures offers several key advantages. First, PCMs can adaptively conform to complex and non-planar heat sources, improving device flexibility and interfacial contact.[23] Second, by selecting PCMs with tailored phase transition temperatures, excessive heat in high-temperature environments can be absorbed, thereby protecting semiconductor components and extending device lifetime.[24] Third, the inherent heat storage and release characteristics of PCMs provide a stable thermal input under fluctuating heat conditions, significantly enhancing output stability and reliability.[25] Unlike conventional studies that primarily focus on intrinsic material optimization, this work emphasizes steady-state operation and environmental adaptability at the device level, thereby tightly linking efficiency enhancement with practical applicability. In recent years, diverse PCM systems—such as graphene-based composites,[26] lignin-g-polycaprolactone systems,[27] and bio-based PCMs derived from spent coffee grounds[28] and building-integrated composites[29]—have been developed, highlighting the multifunctionality of PCMs in thermal management. Early attempts to couple PCMs with TEGs showed promise but did not comprehensively address the challenges of low efficiency at low or high temperatures, unstable output, and short discharge durations.[30]

Here, we present an integrated approach that directly embeds TEG units within composite PCMs, forming a novel PCM-TEG system (Scheme 1). This challenging integration strategy involves fabricating a flexible, series-connected thermoelectric p–n junction matrix, which is subsequently embedded in a sandwich-like structure composed of two form-stable PCMs, 50 wt% hexadecane and 30 wt% stearic acid encapsulated in silicone, arranged vertically. The phase transition temperatures of these materials are 21.58 °C and 76.07 °C, respectively. The resulting integrated device resembles a sandwich structure encapsulated between two phase-change points. This architecture transforms passive thermal storage into active energy conversion, uniting efficient heat storage with continuous electricity generation. By incorporating thermally conductive electrodes into multi-layered composite PCMs, the system preserves thermal storage capacity while stabilizing electricity output under fluctuating heat input. This strategy tackles the fundamental challenges faced by TEGs under

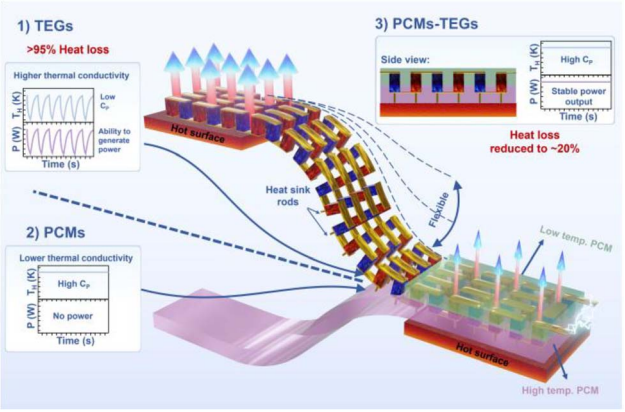

Scheme 1 The diagram of PCM-TEG design.

thermally unstable operating conditions, including low efficiency, operational instability, and limited-service life. Our results demonstrate a reduction in instability from 92% to below 15%, a doubling of effective power output (11.25 W m^{-2} to 23.13 W m^{-2}), and a >500% improvement in operational lifetime. Collectively, these advances establish the PCM-TEG as a robust paradigm for sustainable thermoelectric battery systems, offering broad applicability in energy storage, waste-heat recovery, and thermal insulation technologies.

Experimental

Materials and treatment process

High-performance n-type and p-type Bi_2Te_3 thermoelectric material pellets (1.4 × 1.4 × 1 mm size, metal nickel plated on one side) and 1 × 1 cm, 4 × 4 cm thermoelectric generator devices were purchased from Hubei Segui Energy Technology Company. For temperature degradation tests, n-type, p-type thermoelectric pellets and TEG devices were placed in an oven at 60 °C (24 hours), 150 °C (24 hours), 170 °C (3 hours), 200 °C (1 hour), and 300 °C (1 hour). Conductive material copper foil and low temperature solder (210 °C) were purchased from RS Components Singapore. PlatSil® 73–20 Silicone Rubber (two-part system, Part A and Part B) was purchased from Polytek Development Corp. Stearic acid of purity 95% and hexadecane of 99% purity were purchased from Sigma-Aldrich. All chemicals were used without further purification.

PCM layer preparation

The PCM layers were prepared by the same method in our previous work.[31] The silicone matrix was fabricated using PlatSil® 73–20 Part A : Part B with a weight ratio of 1 : 1. The 70 °C PCM layer (PCMh) was prepared by mixing PlatSil® 73–20 Part A : Part B : stearic acid in a weight ratio of 3.5 : 3.5 : 3, while the 20 °C PCM layer was mixed in a weight ratio of PlatSil® 73–20 Part A : Part B : hexadecane 2.5 : 2.5 : 5. In brief, the respective PCM (stearic acid or hexadecane) was mixed homogeneously with PlatSil® 73–20 Part B, followed by PlatSil® 73–20 Part A. The mixture was then poured into a mold and cured at room temperature overnight.

Device fabrication

The flexible thermoelectric device was constructed by arranging p-type and n-type Bi_2Te_3 pellets in a staggered series configuration, forming a 16 × 16 pellet matrix. To match the dimensions and configuration of commercial devices, homemade flexible devices followed similar dimensions. Upon completion, the thermoelectric device was encapsulated within a bilayer phase change material to complete the final flexible encapsulated device.

Property characterization

Thermogravimetric analysis (TGA) (TA Instruments, Q500) was carried out in an alumina crucible with a nitrogen gas flow rate of 60 mL min^{-1}. Samples were heated from room temperature to 900 °C at a rate of 20 °C min^{-1} to test for the composites' thermal stability. Differential scanning calorimetry (DSC) (TA Instruments, Q100) was performed using aluminum hermetic pans, and heated between −50 and 100 °C at a rate of 10 °C min^{-1} to determine the phase change properties. The specific heat capacity was measured using a differential scanning calorimeter (Mettler Toledo, DSC1). The measurement of thermal diffusivity (D) was carried out on a Netzsch LFA-457 microflash system, and density (ρ) was calculated by measuring the volume and mass at room temperature density, with an experimental error below 1%. XPS measurement was performed on a theta probe angle-resolved X-ray photoelectron spectrometer (ARXPS) system (Thermo Scientific) at a base pressure of 1×10^{-9} Torr and a step size of 0.1 eV using monochromated, micro-focused Al K-Alpha X-ray photons ($h\nu = 1486.6$ eV). The curve fitting and linear background subtraction were carried out using the Advantage software. All the XPS measurements were conducted *ex situ* to evaluate the chemical state of the materials after exposure to real-world operating conditions. *ZT* is the most critical and commonly used parameter to measure the comprehensive performance of TEG devices. Since there is no general and commercial *ZT* measurement equipment, our team customized a *ZT* measurement system based on the Harman effect (SI) that can accurately measure completed thermoelectric samples at room temperature, as shown in Fig. S1.

We developed a customized thermoelectric device power output dynamic test system. We designed and set up a custom system to evaluate the power output of TEG devices under real-world temperature fluctuations. Its key components include: (i) heat source contact platform: precisely controls the contact area between the heat source and the TEG device, enabling simulation of variable temperature conditions. (ii) Keithley 2400 Source Meter: captures and records power output data, connected to a computer for control and analysis.

Results and discussion

Device reliability and degradation

Enhancing thermal reliability and mitigating performance degradation remain critical challenges in the development of TEGs, as these factors directly determine conversion efficiency, operational lifetime, and applicability in diverse waste-heat recovery scenarios.[32] A fundamental understanding of degradation mechanisms is therefore essential for advancing the practical application of TEGs.

To evaluate thermal stability under continuous operation, we fabricated 4 × 4 unencapsulated commercial TEG devices composed of exposed n-type and p-type Bi_2Te_3 pellets. The devices were tested on a heated platform maintained at 120 °C (Fig. 1a). A conventional aluminum heat sink was applied at the cold end to simulate a minimal thermal management configuration. As shown in Fig. 1b, the open-circuit voltage (V_{oc}) exhibited an initial sharp decline, decreasing by ~85% relative to its peak before gradually stabilizing. This transient behavior can be attributed to the system approaching thermal equilibrium, wherein the temperature gradient across the TE legs becomes steady. Nevertheless, the actual power output reached only ~5% of the theoretical maximum, underscoring the severe inefficiency of this unprotected setup.

More importantly, irreversible degradation was observed under prolonged operation. As shown in Fig. 1c, the device failed after ~6 days of continuous testing, reflecting material instability, surface oxidation, and possible mechanical fatigue at electrode interfaces. These results highlight the inherent vulnerability of unencapsulated Bi_2Te_3-based TEGs to long-term thermal exposure. This raises a central question: can encapsulation strategies effectively suppress thermal degradation and extend device reliability?

Thermal degradation in commercially packaged TEGs

First, we used commercial packaging to encapsulate TEGs. Interestingly, a similar attenuation effect was observed even in commercially fabricated and encapsulated TEGs. As shown in Fig. 2a, exposure to temperatures above 200 °C resulted in visible discoloration and structural deterioration of the device packaging. This observation demonstrates that packaging alone is insufficient to prevent high-temperature degradation, necessitating closer evaluation of device-level performance under thermal stress.

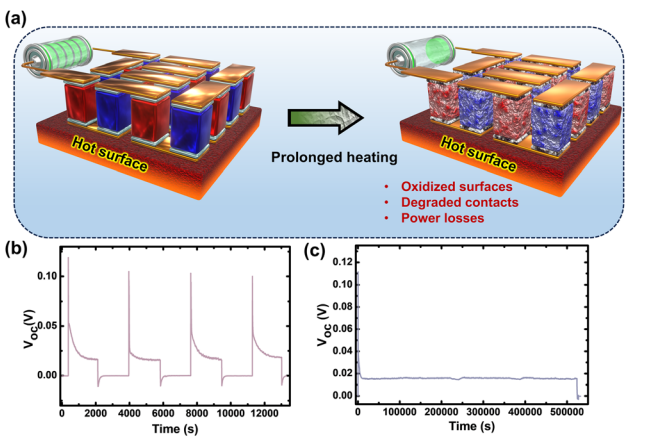

Fig. 1 Thermal instability and performance degradation of unencapsulated TEGs. (a) Schematic illustration of the thermal decay process in an unencapsulated TEG. (b) Evolution of the open-circuit voltage (V_{oc}) under repeated thermal cycling. (c) Long-term V_{oc} degradation curve under continuous operation.

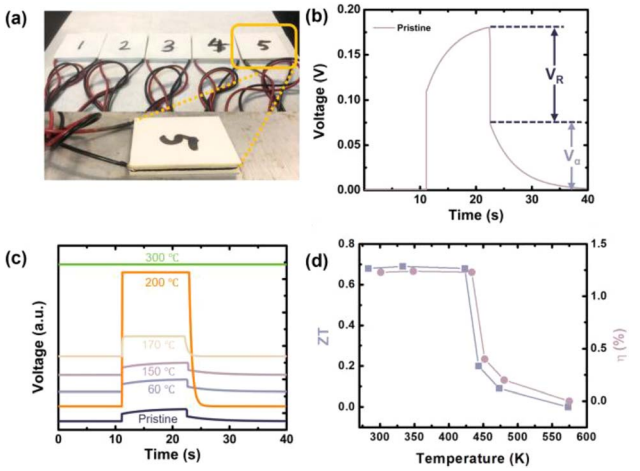

Fig. 2 Performance degradation and thermal sensitivity of commercial thermoelectric generators (TEGs). (a) Optical image of five TEG samples stored at different temperatures: sample 1 (60 °C, 24 h), sample 2 (150 °C, 24 h), sample 3 (170 °C, 3 h), sample 4 (200 °C, 1 h), and sample 5 (300 °C, 1 h). (b) Harman-effect-based *ZT* characterization of a pristine TEG, showing voltage response and the extraction of V_R and V_α. (c) Voltage response of TEGs subjected to stepwise hot-side temperatures. (d) Temperature dependence of *ZT* and conversion efficiency (η), showing pronounced degradation at elevated temperatures.

Because thermal reliability remains a fundamental barrier to practical deployment, it is essential to assess TEGs under realistic and dynamic operating conditions. Conventional characterization methods typically isolate thermal and electrical measurements to estimate the *ZT*, but these approaches are labor-intensive and provide limited insight into the integrated behavior of complete devices. To address this limitation, we developed a custom Harman-effect measurement platform for direct *ZT* characterization at the device level (Fig. S1). The Harman effect, which arises from voltage generation under an induced temperature gradient, enables a representative evaluation of overall thermoelectric performance. By measuring V_R and V_α, the *ZT* of the entire device was obtained using eqn S2 (Fig. 2b). The resulting *ZT* and efficiency curves (Fig. 2c and d) identify 150 °C as a critical thermal threshold, beyond which both conversion efficiency and long-term reliability degrade sharply, underscoring the thermal sensitivity of packaged TEGs. After continuous thermal exposure for several weeks at temperatures up to 130 °C, the V_{oc} and *ZT* values showed negligible changes (less than 5% fluctuation), and the performance was fully repeatable upon cooling and reheating, as shown in Fig. S2.

This instability and irreversible degradation can be attributed to the interplay of intrinsic material vulnerabilities and device-level design constraints. Likely mechanisms include: (i) mechanical stress: cyclic thermal expansion and contraction induce internal stresses, leading to cracking or delamination. (ii) Thermal oxidation: oxidation and element migration occur in both p-type and n-type TE materials at elevated temperatures. (iii) Phase transitions: structural changes at high temperatures disrupt electrical and thermal transport properties. Together, these findings highlight the urgent need for integrated packaging and thermal management strategies that move beyond conventional encapsulation to ensure reliable long-term operation.

Thermal oxidation of materials

The irreversible decline in device efficiency under high-temperature operation strongly suggests intrinsic thermal oxidation of the TE materials themselves. Since the *ZT* directly dictates TEG performance, elucidating the thermal stability and chemical reliability of the constituent p-type and n-type compounds is critical for extending device longevity.[33]

To probe oxidation pathways at the material level, we employed X-ray Photoelectron Spectroscopy (XPS), a high-resolution technique capable of detecting oxidation states and chemical bonding configurations with high precision.[34] This method enables direct monitoring of compositional and electronic structure changes induced by thermal stress. As shown in Fig. 3, p-type Bi_2Te_3 exhibited pronounced temperature-dependent alterations in both elemental composition and oxidation states. Progressive oxidation was observed upon exposure to elevated temperatures, particularly within the Bi 4f and Te 3d spectral regions, revealing the emergence of Bi–O and Te–O bonding. These spectral shifts confirm the breakdown of the parent compound structure and the onset of chemical instability. Such chemical oxidation severely compromises carrier transport and alters thermal conductivity, resulting in a marked reduction in *ZT* and overall device efficiency. These findings reveal the fundamental limitations of current Bi_2Te_3-based materials under prolonged high-temperature operation and underscore the urgent need for stabilization strategies, including encapsulation, protective interfacial coatings, or the development of thermoelectric compounds with intrinsically greater thermal robustness.

XPS revealed a previously unrecognized early-stage thermal oxidation pathway in p-type Bi_2Te_3, initiating at temperatures as

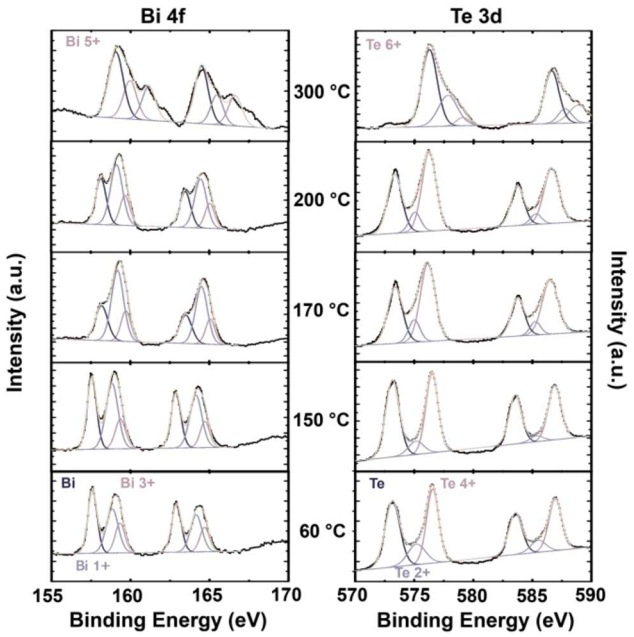

Fig. 3 XPS spectra of Bi 4f and Te 3d recorded before and after oxidation experiments on a p-type Bi_2Te_3-based sample at 60 °C, 150 °C, 170 °C, 200 °C, and 300 °C.

low as 170 °C. Whereas prior studies typically report an oxidation onset above 250 °C,[35] our results demonstrate the formation of high-valence oxidation states at substantially lower temperatures, underscoring the intrinsic thermal vulnerability of Bi_2Te_3-based compounds. In the Bi 4f spectrum, emergent Bi^{5+} signals were detected alongside the commonly reported Bi^{+} and Bi^{3+} species, indicating a more aggressive oxidation pathway than previously acknowledged. At 300 °C, the Te 5d spectrum further confirmed oxidation through the appearance of Te^{6+} peaks, evidencing deep chemical restructuring rather than superficial surface oxidation. These transformations compromise both carrier transport and thermal conductivity, leading to an inevitable reduction in *ZT* and device efficiency.

Strikingly, n-type Bi_2Te_3 exhibited even greater sensitivity. As shown in Fig. S3, highly oxidized Bi^{5+} and Te^{6+} states emerged at only 150 °C, well below the oxidation threshold of p-type samples. This asymmetry implies that the thermal operating ceiling of n-type elements dictates the safe limit of p–n pair-based TEG systems, effectively capping long-term stability at ≤150 °C. For metal alloys, the chemical Bi 4f and Te 3d of metallic elements are both represented by two sets of XPS peaks, corresponding to two distinct metal ion states. However, as temperature increases, the metal ion peaks shift entirely toward higher binding energies. This indicates that both metals exhibit new chemical states, specifically those characteristics of metal oxide peaks. Thus, the destruction of the original alloy systems gives rise to new chemical states—metal oxide states. This signifies that the alloy materials undergo varying degrees of temperature-dependent oxidation reactions and thermal degradation. XPS analysis further shows that sample 10–20 nm also exhibits clear signs of oxidation, although not as pronounced as in the surface layer (Fig. S6). Furthermore, TGA analysis indicates that the material is highly stable at room temperature through 300 °C and shows no loss in mass (Fig. S7). AS a result, the oxidation is occurring at a dilute molecular level.

These findings establish an early-onset oxidation mechanism in the Bi_2Te_3 thermoelectric, far earlier than previously recognized, with profound implications for practical TEG applications under fluctuating or elevated thermal environments. Despite extensive research into high-*ZT* materials, effective strategies for suppressing such oxidation remain scarce. Potential approaches include: (i) surface passivation layers, *e.g.*, inert coatings to suppress oxygen ingress.[36] (ii) Vacuum encapsulation or hermetic sealing, to minimize oxidative exposure.[37] (iii) Material innovation, focusing on intrinsically more thermally robust TE compounds.[38]

Transient thermal fluctuations and interface stability

Beyond chemical oxidation, our results highlight a broader operational limitation: the reliance of the Seebeck effect on a stable and sustained temperature gradient. In practice, fluctuations arising from unsteady heat sources or interfacial thermal resistance induce erratic output, parasitic heat leakage, and reduced conversion efficiency. *ZT* characterization of the thermoelectric devices revealed an exceptionally rapid thermal response (<50 ms), confirming the intrinsic sensitivity of the Seebeck effect to temperature variations.[39,40] While such responsiveness is advantageous for harvesting dynamic heat flux, it simultaneously renders TEGs highly vulnerable to transient fluctuations in heat supply, often leading to abrupt performance collapse.[41]

To systematically probe this behavior, we employed a custom-designed testing platform that periodically alternated contact and separation between the heat source and the TEG interface (Fig. 4a). A 1 : 2-time ratio between separation and contact was maintained to emulate unstable heat delivery conditions. During a 10 s separation from a 60 °C heat source, the hot-side temperature decreased from 56.5 °C to 48.5 °C, accompanied by a sharp drop in V_{oc} from 0.28 V to 0.072 V, corresponding to a 74% reduction. More critically, the output power decreased by 92%, underscoring the severe impact of transient thermal disturbances on device performance. Upon restoring thermal contact, device parameters recovered to near-maximal values within ~20 s, and this recovery behavior was highly reproducible across ten consecutive cycles (Fig. 4b).

These results highlight a critical challenge: thermoelectric efficiency is inherently unstable under fluctuating temperature gradients, a factor often overlooked in conventional performance evaluations. Importantly, instability at the heat source–TEG interface not only induces immediate efficiency loss but also accelerates long-term material oxidation, as repeated thermal cycling exacerbates oxidation, mechanical fatigue, and contact failure. Taken together, these findings establish interface temperature stability as a unifying prerequisite for overcoming the dual bottlenecks of material-level oxidation and device-level unreliability, thereby guiding the design of robust, real-world thermoelectric systems. Addressing these challenges requires a dual-level strategy: (i) material stabilization, through compositional design and protective engineering, and (ii) system-level thermal management, employing advanced thermal interface materials (TIMs), PCM-based thermal buffers, or active regulation schemes. A holistic integration of these approaches is essential to realize durable, high-performance TEGs and to unlock their potential as long-term solutions for waste-heat recovery across industrial, automotive, and wearable applications.

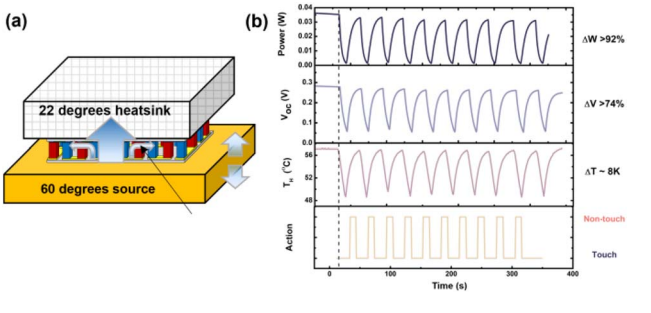

Fig. 4 Evaluation of TEG performance under unstable heat source conditions. (a) Schematic of the custom measurement setup simulating hot-end instability by periodically separating and re-establishing contact between the heat source and the TEG interface. (b) Time-dependent variations of hot-side temperature (TH), open-circuit voltage (V_{OC}), and output power.

Interface redesign using phase-change materials

To mitigate the thermal instability and mechanical fragility of conventional thermoelectric devices, we redesigned the device interface by replacing rigid ceramic substrates with a soft, thermally stable interfacial material. This multifunctional design confers three distinct advantages: (i) thermal buffering – the interfacial material's low thermal conductivity and high thermal capacitance suppress rapid thermal transients, shielding thermoelectric elements from abrupt temperature shocks. (ii) Encapsulation and protection – acting simultaneously as an interface and encapsulant, the material minimizes parasitic heat loss while protecting the device against oxidation, diffusion, and environmental degradation. (iii) Enhanced conformability – its inherent flexibility enables intimate thermal contact with non-planar or curved heat sources, thereby improving interfacial heat transfer.

PCMs were identified as optimal interface candidates owing to their large latent heat capacity and tunable transition temperatures. To hold the two ends of the TEGs at a suitable temperature gradient, hexadecane and stearic acid were chosen as PCMs to be encapsulated by a silicone-based matrix (Plat-Sil®) to form form-stable PCMs. 30 wt% of stearic-acid was loaded into the silicone matrix to give a composite material with a melting point of 76.07 °C and latent heat of 43.62 Jg^{-1}, which was assigned as the hot-side PCM (PCMh). However, 50 wt% hexadecane in the silicone matrix gave a melting point of 21.58 °C and latent heat of 73.50 Jg^{-1}, which was assigned to the cold end of the TEGs (PCMc) (Fig. 5a). Both form-stable PCMs exhibited good thermal stability at the maximum TEG operating temperature, where thermal degradation to 98 wt% approximately occurred above 139 °C (Fig. 5b). In addition, both PCMh and PCMc demonstrated excellent thermal cycling stability over 100 heating–cooling cycles (Fig. S4). Although minor evolution in the DSC curve shape was observed during the initial cycles, it is probably due to microstructural rearrangement and stabilization of the PCM domains within the silicone matrix.[42] Importantly, the latent heat remained highly stable, with variations below 0.6% for PCMh and 0.2% for PCMc, confirming negligible degradation and reliable long-term thermal performance. As shown in Fig. S5a, integrating a hot-side PCM with a transition temperature of 76.07 °C effectively confined the TEGs' hot-end temperature within a narrow 60–70 °C range, even under a 100 °C heat source. This thermal buffering not only stabilized the input conditions but also enhanced the device's safety and operational durability. During stability testing, the thermal stability of the PCM outperformed the baseline stability of the TEG modules themselves under the tested conditions, with no observable leakage or significant degradation in latent heat performance.

Employing a tandem PCM configuration, with 76.07 °C PCM positioned on the hot side and a 21.58 °C PCM on the cold side, resulted in a remarkably stable voltage output under dynamic thermal conditions (Fig. S5b). This approach validates the PCM-TEG concept, wherein PCMs function as bidirectional heat reservoirs that smooth temperature gradients and extend TEG reliability. Critically, when benchmarked against conventional devices without PCM encapsulation, the PCM-integrated TEGs exhibited a >500% improvement in stability and a twofold enhancement in effective power output. This direct comparison highlights that the incorporation of PCMs not only buffers thermal shocks but also provides a robust pathway to overcoming the long-standing challenges of oxidation and unstable operation.

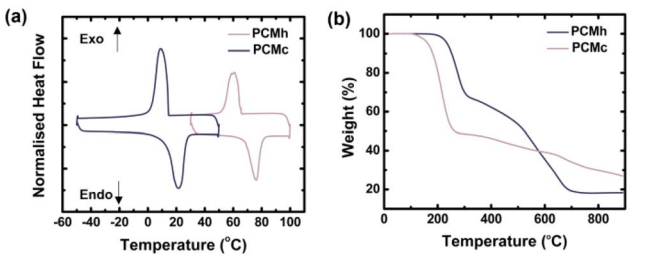

Fig. 5 Characterization of PCM characteristics. (a) The DSC curves for PCMh and PCMc. (b) The TGA curves of PCMh and PCMc.

Fabrication of a flexible PCM-TEG system

Building upon these interfacial insights, we fabricated a flexible PCM-TEG device (Fig. 6a), encapsulating the thermoelectric core within a tandem PCM framework. The PCMh (76.07 °C) layer beneath and the PCMc (21.58 °C) layer above act synergistically as dual thermal buffers, simultaneously stabilizing the thermal gradient and protecting the TE materials (Fig. 6b). To demonstrate the integration of soft PCMs with thermoelectric devices, the PCM is designed into an interlocking structure, as shown in Fig. S8a. Fig. S8b illustrates that this soft PCM can naturally conform to the curved surface of a heat source, achieving seamless contact. Consequently, when heated, the thermoelectric device can efficiently and steadily exchange heat with the source through this conformal PCM layer, as depicted

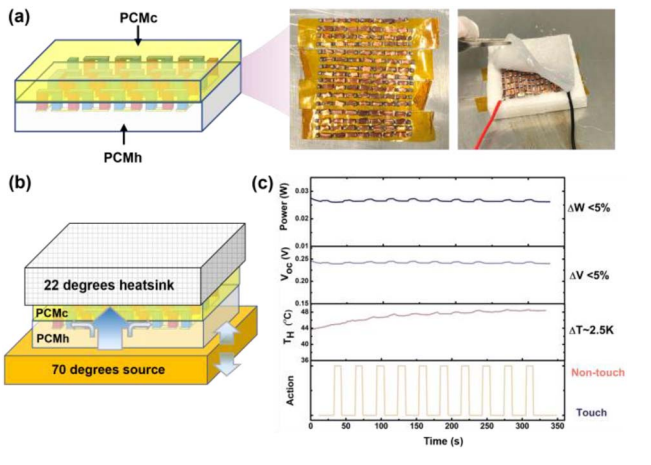

Fig. 6 Performance evaluation of the flexible PCM-TEG device under unstable thermal conditions. (a) Fabrication of a 16 × 16 thermoelectric matrix (40 × 40 mm) by connecting p-type and n-type Bi_2Te_3 pellets in series. (b) Schematic of the test configuration simulating hot-end instability through repeated contact and separation between the heat source and the PCM-TEG interface. (c) Time-resolved measurements of hot-side temperature (TH), open-circuit voltage (V_{OC}), and output power, demonstrating stabilized performance.

in Fig. S8c. This architecture enables the co-integration of stable thermal energy storage with active thermoelectric generation, yielding a high-performance, mechanically flexible thermoelectric battery. The resulting PCM-TEG system delivers sustained power output with markedly reduced degradation, while exhibiting broad adaptability across diverse application scenarios, including wearable electronics, industrial waste-heat recovery, and solar-thermal energy harvesting.

To evaluate real-world applicability, the flexible PCM-TEG system was tested using the custom unsteady heat source measurement platform described previously. In contrast to earlier results (Fig. 4), where unbuffered TEGs exhibited sharp thermal spikes and severe voltage collapse, the redesigned device incorporating a composite tandem PCM interface demonstrated remarkable resilience to fluctuating thermal inputs. During cyclic heating, the hot-side temperature rose gradually and stabilized at ~48 °C, even under intermittent source contact. Importantly, the temperature difference across the device was tightly maintained within a narrow 2.5 °C window, representing a substantial improvement over the highly erratic thermal profiles observed in the unencapsulated configuration. This stabilization translated directly into exceptionally stable electrical performance. The open-circuit voltage remained constant at ~0.24 V with fluctuations below 5%, while the device delivered a steady power output of 0.026 W with a similar variability of <5%. Such stability marks a paradigm shift in thermoelectric design: the PCM-TEG system functions not only as a power generator but also as a thermoelectric battery, simultaneously storing and converting thermal energy to deliver reliable performance in dynamic environments (Fig. 6c).

Nevertheless, a modest reduction in peak V_{oc} and maximum power was observed compared to conventional unencapsulated devices. Two factors contribute to this effect: (i) the limited thermal conductivity of the PCM layer, which restricts heat flux into the TE junction. (ii) The reduced overall temperature gradient across the device due to the thermal buffering action of the PCMs. These trade-offs are quantitatively described by eqn S4 (SI), underscoring the inherent balance between peak power output and operational stability. Despite this modest reduction, the benefits of long-term reliability, stable performance, and enhanced material protection far outweigh the loss in maximum instantaneous efficiency, particularly for applications where consistent energy delivery under fluctuating conditions is essential, such as waste-heat recovery, wearable energy harvesters, and off-grid power systems.

Enhancing hot-end temperature control *via* thermally conductive pins

Maintaining structural integrity in tandem PCM architectures while ensuring precise hot-end temperature control represents a critical engineering challenge. To address this limitation, we embedded high-conductivity copper wires, referred to as thermally conductive pins, into the hot-side copper electrode (Fig. 7a). Acting as localized thermal conduits, these pins reduce the internal temperature gradient across the PCMh, thereby enabling the thermoelectric module to operate closer to its optimal thermal differential.

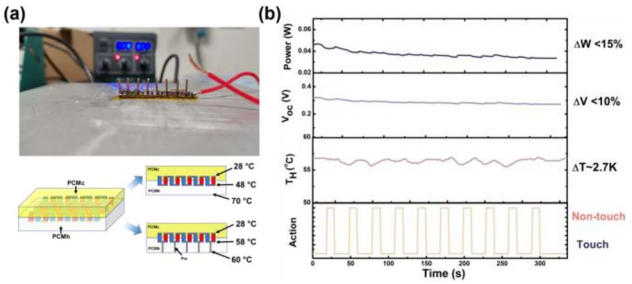

Fig. 7 Enhanced thermal regulation of the PCM-TEG using embedded copper conductive pins. (a) Schematic illustration of the modified PCM-TEG-pin device, where copper wires are introduced to improve the thermal conductivity of the high-temperature PCM layer and stabilize hot-end temperature under fluctuating heat input. (b) Time-resolved profiles of hot-side temperature (TH), open-circuit voltage (V_{oc}), and power output.

The benefits of this modification are evident in Fig. 6b. With conductive pins, the hot-side temperature stabilized at 58 °C with fluctuations of only 2.7 °C, compared to the ~48 °C peak observed in devices without pins. This improvement directly translated into enhanced electrical performance: V_{oc} increased to 0.31 V. Maximum power output exceeded 0.04 W (Fig. 7b). Beyond improving peak output, the integration of conductive pins endowed the device with resilience against heat-source interruptions. The PCMh layer, functioning as a thermal battery, gradually released stored latent heat, sustaining power generation even in the absence of active heating. This buffering capability prevented abrupt voltage collapse and mitigated risks associated with sudden shutdowns.

This uninterrupted energy conversion capability marks a distinct advantage over conventional TEGs. By ensuring both thermal regulation and continuous energy delivery, the conductive pin-integrated PCM-TEG system achieves superior operational reliability and energy efficiency. In summary, while the tandem PCM framework establishes long-term thermal stability and reliability, the addition of thermally conductive pins recovers peak temperature differentials and boosts maximum power output. Together, these complementary strategies deliver a PCM-TEG architecture that simultaneously addresses stability and performance—two of the most critical challenges in practical thermoelectric energy harvesting.

Conclusions

This work provides a comprehensive investigation into the degradation pathways and reliability challenges of TEGs under high temperatures and unstable heat sources. We demonstrated that premature oxidation, thermal instability, and insufficient encapsulation critically undermine long-term performance. To overcome these barriers, we developed a flexible PCM-TEG system that integrates dual phase-change materials (PCMh and PCMc) within a tandem encapsulation framework. This architecture transforms conventional rigid TE devices into multifunctional, self-regulating converters capable

of simultaneously storing thermal energy and stabilizing thermal gradients.

The proposed design achieved substantial improvements, reducing device instability from 92% to below 15%, increasing the effective power output by over 100% (up to 23.13 W m^{-2}), and enhancing thermal durability by more than fivefold under prolonged high-temperature operation (Table S1). The calculated device-level conversion efficiency showed a relative improvement of 170% and 350% due to the optimized thermal impedance matching provided by the PCM and PCM with copper-pin architecture. These achievements underscore the central role of thermal interface engineering in addressing both short-term efficiency and long-term reliability.

Beyond immediate performance gains, this study underscores a broader design principle – coupling thermal buffering with active energy conversion to achieve resilient operation under thermally volatile conditions. By bridging material-level stabilization with system-level thermal management, the PCM-TEG paradigm provides a robust pathway toward practical, scalable deployment of thermoelectric in waste heat recovery, off-grid energy supply, and wearable electronics. Ultimately, this work establishes a foundation for next-generation thermoelectric technologies, where stability and efficiency are co-optimized – a prerequisite for translating laboratory performance into real-world sustainability solutions. One of future iterations will focus on the synthesis of eutectic salt-matrix composite PCMs.

Author contributions

X. W. conceived and coordinated the study. W. C. and X. Y. D. S. analyzed the data and wrote the paper. J. D., X. Y. T., and S. W. synthesized and characterized the materials. W. T., R. J., J. X., and X. J. L. performed the experiments. W. C. and X. W. discussed the results, interpreted the data, and revised the paper. Y. Z., H. Y., and Q. Z. supervised the research.

Conflicts of interest

There are no conflicts to declare.

Data availability

The data that support the findings of this study are available from the corresponding author upon reasonable request.

Supplementary information (SI) is available. See DOI: https://doi.org/10.1039/d6ta00496b.

Acknowledgements

The authors are grateful for the financial support from MOE ACRF Tier 1 RG128/21 and Singapore A*STAR project A19D9a0096 and A*STAR RIE 2025-International Relations Grant Ref Number R24I5IR046 and National Research Foundation (NRF) Singapore under its NRF Investigatorship (NRF-NRFI07-2021-0003) and Program of China Scholarship Council (Grant No. 202506290002). This research is also supported by the National Research Foundation, Singapore, and National Environment Agency, Singapore under its Closing the Resource Loop Funding Initiative (Award No. CTRL-2025-1R-15).

Notes and references

1 B. C. Gibb, *Nat. Chem.*, 2025, **17**, 629–631.
2 B. Nan, G. Xu, Q. Yang, B. Zhang and X. Zhou, *Energy Convers. Manage.*, 2023, **283**, 116880.
3 K. Liu, J. Wang, X. Pan, S.-Y. Tian, Y. Liu, Z. Zhang, Y. Di, J. Chen, C. Wu, X.-Y. Deng, D. Wang, P. Li, C.-K. Pan, F. Qi, J. Liu, J. Hua, J. Pei, C.-a. Di, Y. Guo, Y. Liu and T. Lei, *Nature*, 2025, **644**, 920–926.
4 V. Taneja, S. Mishra, U. V. Waghmare and K. Biswas, *ACS Energy Lett.*, 2025, **10**, 3866–3875.
5 J.-Z. Liu, S.-Q. Chen, Y.-Y. Ju, M.-P. Zhuo and K.-Q. Zhang, *Mater. Today*, 2025, **88**, 585–596.
6 H. Xu, J. Wang, Y. Zhou and H. Jiang, *Energy*, 2024, **308**, 132973.
7 B. Anya, M. Mohammadpourfard, G. G. Akkurt and B. Mohammadi-Ivatloo, *Renew. Sustain. Energy Rev.*, 2025, **210**, 115185.
8 J. Hong, J. Song, U. Han, H. Kim, H. Choi and H. Lee, *eTransportation*, 2024, **20**, 100317.
9 K. Biswas, J. He, I. D. Blum, C.-I. Wu, T. P. Hogan, D. N. Seidman, V. P. Dravid and M. G. Kanatzidis, *Nature*, 2012, **489**, 414–418.
10 G. J. Snyder and E. S. Toberer, *Nat. Mater.*, 2008, **7**, 105–114.
11 L.-D. Zhao, S.-H. Lo, Y. Zhang, H. Sun, G. Tan, C. Uher, C. Wolverton, V. P. Dravid and M. G. Kanatzidis, *Nature*, 2014, **508**, 373–377.
12 Z. Zhao, J. Zheng, Y. Li, S. Wang, S. Liu, S. Zhan, L. Wang, X. Zhang and L.-D. Zhao, *Nano Energy*, 2024, **126**, 109649.
13 L. Wang, A. Li, X. Wu, J. Li, T. Ohsawa and T. Mori, *Adv. Mater.*, 2025, **37**(38), 2508270.
14 J. H. Kim, J. H. Yun, S. H. Cha, S. Byeon, J. Park, H. Jin, S. Kim, S. J. Kim, J. Park, J. Jang, S. Park and J. S. Rhyee, *Adv. Funct. Mater.*, 2024, **34**, 2404886.
15 E. Godlewska, K. Zawadzka, A. Adamczyk, M. Mitoraj and K. Mars, *Oxid. Met.*, 2010, **74**, 113–124.
16 Y. Wang, X. Zhang, Y. Wang, H. Liu and J. Zhang, *Phys. Status Solidi*, 2019, **216**, 1800811.
17 P. Balasubramanian, M. Battabyal and R. Gopalan, *Mater. Lett.*, 2022, **312**, 131599.
18 C. Jiang, X. a. Fan, Z. Rong, C. Zhang, G. Li, B. Feng, J. Hu and Q. Xiang, *J. Electron. Mater.*, 2017, **46**, 1363–1370.
19 H. Zhou, X. Mu, W. Zhao, D. Tang, P. Wei, W. Zhu, X. Nie and Q. Zhang, *Nano Energy*, 2017, **40**, 274–281.
20 D. Music, K. Chang, P. Schmidt, F. N. Braun, M. Heller, S. Hermsen, P. J. Pöllmann, T. Schulzendorff and C. Wagner, *J. Phys.: Condens. Matter*, 2017, **29**, 485705.
21 J. Li, J. Lyu, W. Yang, Z. Ren, Z. Chen, Z. Zhao, J. Jiang, H. Yang and J. Shuai, *Small*, 2024, **20**, 2311340.
22 H. Ming, Z.-Z. Luo, Z. Zou and M. G. Kanatzidis, *Chem. Rev.*, 2025, **125**, 3932–3975.

23 T. W. Luo, L. L. Kong, J. J. Lu, M. Xie, B. F. Lin, L. H. Fu, B. Huang and C. H. Xu, *Adv. Mater.*, 2024, **36**, 2411820.
24 T. Lo Wong, C. Vallés, A. Nasser and C. Abeykoon, *Renewable Sustainable Energy Rev.*, 2023, **187**, 113730.
25 Z. F. Wang, S. X. Liu, C. Z. Zhu and J. Xu, *Adv. Mater.*, 2024, **36**(30), 2403889.
26 R. C. Li, X. X. Sun, R. Zhang, S. S. Wang, Q. Q. Liu, P. J. Bai, Y. Yuan and Y. B. Li, *Chem. Eng. J.*, 2025, **504**, 158964.
27 J. J. C. Lee, S. Sugiarto, P. J. Ong, X. Y. D. Soo, X. P. Ni, P. Luo, Y. Y. K. Hnin, J. S. Y. See, F. X. Wei, R. Y. Zheng, P. Wang, J. W. Xu, X. J. Loh, D. Kai and Q. Zhu, *J. Energy Storage*, 2022, **56**, 106118.
28 P. J. Ong, Y. Leow, X. Y. D. Soo, M. H. Chua, X. Ni, A. Suwardi, C. K. I. Tan, R. Zheng, F. Wei and J. Xu, *Waste Manage.*, 2023, **157**, 339–347.
29 P. J. Ong, Y. Y. Lum, X. Y. D. Soo, S. Wang, P. Wang, D. Chi, H. Liu, D. Kai, C.-L. K. Lee and Q. Yan, *Constr. Build. Mater.*, 2023, **386**, 131583.
30 K. K. Chen, X. Chen, Y. Li, Y. H. Feng, X. F. Li, Z. Q. Li, S. M. Liu and C. H. Ge, *J. Energy Chem.*, 2025, **107**, 548–557.
31 X. Y. D. Soo, Z. M. Png, M. H. Chua, J. C. C. Yeo, P. J. Ong, S. Wang, X. Wang, A. Suwardi, J. Cao, Y. Chen, Q. Yan, X. J. Loh, J. Xu and Q. Zhu, *Mater. Today Adv.*, 2022, **14**, 100227.
32 L. Miao, Q. Zhang, M. Yuan, R. Li, M. Wang, X. Tan, J. Wu, G.-Q. Liu and J. Jiang, *Adv. Mater.*, 2025, **37**, 2503580.
33 A. F. Ioffe, L. S. Stil'bans, E. K. Iordanishvili, T. S. Stavitskaya, A. Gelbtuch and G. Vineyard, *Phys. Today*, 1959, **12**, 42.
34 W. Chen, S. Zhong, Q. Cai, Z. Jiang, Q. Hu, C. Tang, Q. Zhao, Z. Wang, S. Wang, X. Zheng, F. Liang, H.-D. Yu and L. Li, *Matter*, 2025, **8**, 102088.
35 C. Jiang, X. a. Fan, B. Feng, J. Hu, Q. Xiang, G. Li, Y. Li and Z. He, *J. Alloys Compd.*, 2017, **692**, 885–891.
36 S. Z. H. Shah, Z. Aabdin, W. W. Tjiu, W. Nong, J. Recatala-Gomez, V. Chellappan, W. Zhai, D. V. M. Repaka, G. Wu, K. Hippalgaonkar, I. Nandhakumar and P. Kumar, *ACS Appl. Mater. Interfaces*, 2024, **16**, 46191–46199.
37 Y. Tang, Y. Zhang, F. Xing, Y. Qi, Z. Cao, Z. He, J. Zhang and Z. Shi, *Ceram. Int.*, 2025, **51**, 51046–51053.
38 Q. Tang, B. Jiang, K. Wang, W. Wang, B. Jia, T. Ding, Z. Huang, Y. Lin and J. He, *Joule*, 2024, **8**, 1641–1666.
39 W. Zhu, Y. Deng, Y. Wang and A. Wang, *Microelectron. J.*, 2013, **44**, 860–868.
40 U. Birkholz, R. Fettig and J. Rosenzweig, *Sensor. Actuator.*, 1987, **12**, 179–184.
41 M. Fisac, F. X. Villasevil and A. M. López, *Renewable Energy*, 2015, **81**, 658–663.
42 M. M. Kenisarin and K. M. Kenisarina, *Renew. Sustain. Energy Rev.*, 2012, **16**, 1999–2040.